Persistent increases in nighttime heat stress from urban expansion despite heat island mitigation

Kangning Huang[1,2*], Xuhui Lee[1], Brian Stone Jr.[2], Jason Knievel[2], Michelle L. Bell[1], and Karen C. Seto[1]

1. School of the Environment, Yale University, New Haven, CT, USA.
2. Research Application Laboratory, National Center for Atmospheric Research, Boulder, CO, USA.
3. School of City and Regional Planning, Georgia Institute of Technology, Atlanta, GA, USA.

Corresponding author: Kangning Huang (kangning.huang@yale.edu; knhuang@ucar.edu)

Abstract

Urban areas generally have higher near-surface air temperature and lower air humidity than rural areas. Little is known about how heat stress, the combined effect of high air temperature and high humidity on human physiology, will be affected by future urban land expansion. Here we use a mesoscale numerical weather prediction model to examine the effects of urban land expansion from 2000 to 2050 on heat stress (measured as wet-bulb globe temperature, WBGT) in the urban areas of China, India, and Nigeria, which are projected to account for one-third of global urban population growth through 2050. Our results show that urban expansion slightly reduces heat stress during the day (~0.2°C) but substantially intensifies it at night, by ~1°C on average and by up to 2–3°C in five mega-urban regions (MURs). These effects exist with or without climate change induced by rising concentrations of greenhouse gases (GHGs). Installing cool roofs—an urban heat island mitigation measures—can reduce the daytime WBGT by 0.5–1°C, partially offsetting the heat stress conditions caused by GHG-induced climate change. However, even with cool roofs, the nighttime WBGTs are higher by 0.3–0.9°C over the whole countries studied, and by 1–2°C in the MURs under the urban expansion scenario, compared to the situation in which urban areas remain unchanged. These results show that future urban expansion and heat island mitigation can result in potential daytime benefits but also persistent nighttime risks.

1 Introduction

Human bodies cannot effectively cool off through sweating if air temperature and humidity are high, and therefore both variables need to be accounted for in assessing the heat stress on human (Sherwood & Huber, 2010). However, despite a growing body of literature on how both variables are affected by climate change induced by greenhouse gases (GHGs) (Ahmadalipour & Moradkhani, 2018; Fischer & Knutti, 2013; Im et al., 2017; Kang & Eltahir, 2018; J. Li et al., 2018; Matthews et al., 2017; Pal & Eltahir, 2016; Sherwood & Huber, 2010), existing studies on the climatic effects of future urban land expansion primarily focus on rising air temperature (L. Chen & Frauenfeld, 2016; Georgescu et al., 2014; K. Huang et al., 2019; Krayenhoff et al., 2018) but largely overlook changes in humidity. Under humid conditions, while the removal of vegetation by urban expansion raises air temperature by reducing evaporative cooling (Oke, 1982), the reduction of evapotranspiration (ET) also diminishes humidity (Adebayo, 1991; Luo & Lau, 2019; Um et al., 2007) (Figure 1). These warming and drying effects also exist in arid climates, although they as not as pronounced—and sometime inverted—because the ET from native arid/semi-arid vegetation is generally weaker than that from urban green space. In humid climates, previous studies showed that humidity is lower in existing urban areas compared to the surrounding rural areas (Ackerman, 1987; D. O. Lee, 1991), and that the process of urban land expansion can further reduce humidity (Adebayo, 1991; Luo & Lau, 2019). What remains unknown, however, is whether the two opposing processes—warming and drying—associated with future urban expansion will combine to intensify or to weaken heat stress. This question is important in the context of the world's rapidly growing urban population, which is anticipated to reach 6.7 billion by 2050.

Here we combine the Weather Research and Forecasting (WRF) regional numerical weather prediction (NWP) model (Miao & Chen, 2014; Skamarock et al., 2008) and the spatially explicit projections of urban land expansion through 2050 by (K. Huang et al., 2019), to investigate the effects of urban expansion on heat stress intensity. Our index for heat stress is a modified wet-bulb globe temperature (WBGT) at 2m above ground level. Compared to other heat stress indices, heatwaves defined using WBGT have stronger correlations with health impacts (Heo & Bell, 2018). We choose the entire countries of China, India, and Nigeria as the study regions, because one-third of global urban population growth in the next three decades is projected to occur there (UN DESA, 2014), and urban land areas there will expand by 40 million hectares, which is about 27% of the world's total urban land expansion (K. Huang et al., 2019). Heat stress in these regions is projected to rise to dangerous levels due to GHG-induced climate change (Ahmadalipour & Moradkhani, 2018; Im et al., 2017; Kang & Eltahir, 2018), but we do not know if the expected enormous urban expansion will further intensify the heat stress. To examine the possible nonlinear interaction (Krayenhoff et al., 2018) between global climate change and urban expansion, we force the WRF simulations with two sets of background climate conditions: a historical climate in 2000, and a projected climate in 2050 under the representative concentration pathway (RCP) 8.5 scenario (Bruyere et al., 2015; Vuuren et al., 2011). The effects of two infrastructure-based urban heat island mitigations—green and cool roofs installments—are evaluated in additional simulations, to explore a larger range of possible heat stress outcomes in urban areas. By exploring these scenarios, we aim to answer the question of how urban land expansion and heat island mitigation will contribute to changing future heat stress.

2 Methods

2.1 Heat stress calculation.

Our metric for heat stress is a modified wet-bulb globe temperature (WBGT) at 2m above ground level (Dunne et al., 2013):

$$WBGT = 0.7 \times T_w + 0.3 \times T_g$$

wherein T_g is black globe temperature and T_w is natural wet-bulb temperature. Modifying WBGT by ignoring direct sunlight and wind, T_g can be approximated by dry air temperature T_a at 2m. Wet-bulb temperature T_w at 2m can be calculated by solving the equation below (X. Lee, 2018; Monteith & Unsworth, 2013):

$$e = e_s(T_w) - \gamma(T_a - T_w)$$

wherein e is water vapor pressure, $e_s(*)$ is the saturated (i.e. equilibrium) water vapor pressure as a function of temperature, and γ is the psychrometer constant that depends on air pressure and temperature. A numerical method provided in the R package Bigleaf (version 0.6.5) is used to solve T_w (Knauer et al., 2018). Hereafter we omit "modified" when referring to WBGT.

We choose WBGT as the metric for heat stress because it is widely accepted and used (d'Ambrosio Alfano et al., 2014; Blazejczyk et al., 2012). WBGT is used in the fields of industrial hygiene (Lucas et al., 2014), the military (Patel et al., 2013), and sporting (Brocherie & Millet, 2015). More importantly, a recent study comparing different heat stress metrics showed that WBGT is the best indicator of heat-related health impacts, such as hospitalization and heat disorders during heatwaves (Heo et al., 2019).

2.2 Atmospheric modeling.

To simulate the effects of urban land expansion on both air temperature and humidity, we use the advanced research version of the weather research and forecasting model (WRF, version 3.8) coupled with a single-layer urban canopy module (UCM) (D. Li et al., 2014; Miao & Chen, 2014; Skamarock et al., 2008). As a mesoscale physical-based NWP model, WRF can examine the effects of land cover / land use changes—conversion to urban areas from others—on both air temperature and humidity. To provide the initial and boundary conditions for WRF, we use the global bias-corrected climate model output from the Community Earth System Model (CESM), with historical and future GHG concentration (Bruyere et al., 2015). The future climate conditions are based on the Representative Concentration Pathway (RCP) 8.5, which will result from the business-as-usual, fossil-fueled economic development. To account for inter-annual fluctuations, we run the simulations for five summers: 1999–2004 for current climate, and 2049–2054 for future climate. When analyzing the hourly outputs from WRF, we categorize all hours with positive incoming shortwave radiation as daytime, and those with zero shortwave radiation as nighttime. By using incoming shortwave radiation rather than fixed hours to categorize diurnal hours, we account for the different summer daytime lengths across different latitudes. The WRF modeling domains over China, India, and Nigeria are shown in Figure 2.

2.3 Urban land expansion and heat island mitigation.

Future urban areas are obtained from a spatially explicit probabilistic projections of urban expansion by 2050 (K. Huang et al., 2019). The urban expansion in the Shared Socioeconomic Pathway 5 (fossil-fueled development) scenario is used, in order to match with the high emission RCP8.5 climate change scenario. Following (L. Chen & Frauenfeld, 2016), we assume locations with >75% likelihood to be urbanized by 2050 as urban areas. Following previous studies on the climatic impacts of large-scale urban land expansion (L. Chen & Frauenfeld, 2016; Georgescu et al., 2014; Krayenhoff et al., 2018), we run the model at 25 km horizontal grid spacing. We use the global databases of urban extent and characteristics provided by (Jackson et al., 2010) to set up the urban areas' parameters, such as impervious/pervious surfaces ratios, building heights, street widths, heat capacity, and surface albedo. The key urban parameters of the study countries are listed in Table S1. Among the study countries, urban areas in China have the highest height-to-width ratio (1.8), resulting in deeper urban canyons and absorbing of more outgoing longwave radiation compared urban areas in the other two countries. Urban areas in India have the lowest roof albedo, which leads to absorption of more incoming short-wave radiation. Compared to those in India, urban areas in China and Nigeria have higher thermal conductivity, which can increase daytime heat storage and thus stronger nighttime heat release.

We follow (Georgescu et al., 2014) to set up the cool roofs adaptation scenario as the albedo of building rooftops being raised to 0.8. Albedo of building walls and pavements are kept the same in the albedo adaptation scenario, because glare from highly-reflective walls and pavements can cause visibility problems for drivers and pedestrians (Stone, 2012). The green roofs adaptation option is readily available in WRF-v3.8, which includes an UCM that enables modeling vegetation irrigation in urban canyons. Both cool and green roofs adaptations assume a 100% deployment on all available roof tops. Although these adaptations scenarios may not be realistic in terms of implementation, we aim to examine the system boundaries of the urban-climate-adaptation interactions regarding heat stress. Installing green or cool roofs can reduce building energy consumption and thus the anthropogenic heat (AH) released in urban areas. However, this feedback between adaptations and AH is not captured here, because the current version of WRF-UCM does not allow simultaneously simulating building energy use and green roof adaptation (J. Yang, Wang, Chen, et al., 2015). Instead, following (L. Chen & Frauenfeld, 2016; Georgescu et al., 2014), we implement a simple diurnal profile of anthropogenic heating (Figure S2). This implementation of AH may underestimate warming from urban expansion as indoor cooling systems are installed in more buildings, and it may underestimate cooling from urban adaptations as green or cool roofs reduce energy used by indoor cooling. Moreover, this implementation also ignores the spatial heterogeneity of anthropogenic heating, as shown in (F. Chen et al., 2016; B. Yang et al., 2019). To incorporate spatial heterogenous AH in WRF simulations, the input land use data need to include the spatial distributions of urban areas with various densities, which are not available in the urban expansion forecasts (K. Huang et al., 2019). The spatially uniform AH profiles used here may lead to underestimation of warming in the denser areas near city centers.

When presenting the modeling results of changing WBGT in Figure 3, we categorize urban areas into humid and arid. Instead of using the conventional aridity index (the ratio of precipitation to potential evapotranspiration), here we use the difference in summertime average evapotranspiration (ET) before and after urban land expansion to distinguish humid or arid urban areas. If the average ET declines after urban expansion, urban area is removing humidity on an originally humid landscape; on the contrary, if ET increases after urban expansion, urban area is introducing more humidity via urban greenspace that evaporate and transpire more vapor than the native arid vegetation. We use this definition because it can better reflect the different roles urban land expansion play under different climate conditions. The geographic distributions of humid and arid urban areas are shown in Figure 2. When presenting the results across geographies (Figure 4) and on the temperature-humidity-plane (Figure 5), we overlay them on the present Köppen climate zones provided in (Beck et al., 2018). With the labels of Köppen climate zones, we can show which MURs are located in the transition zones (e.g. Beijing and Delhi) and show the differences among various types of humid urban areas.

2.4 Model validation.

To validate the model's capabilities in simulating the diurnal variations of air temperature, humidity, and heat stress, we compare the simulated results with the observations obtained from the integrated surface database (ISD) from the National Oceanic and Atmospheric Administration (Smith et al., 2011). ISD provides hourly meteorological observations with global coverage. In total, 404 ISD stations in China, 408 in India, and 40 in Nigeria are used in the validation. The validation shows that the simulated values agree with the observed ones sufficiently well for air temperature (Figure S4; R^2=0.74), relative humidity (Figure S5; R^2=0.56), and wet-bulb temperature (Figure S6; R^2=0.82). To better evaluate the model's performance in urban areas, the correlation coefficients (R^2's) shown here are calculated with grid cell samples weighted by their fraction of urban land.

3 Results

Our results show that in 2050 urban land expansion and heat island mitigation have diurnally different impacts on WBGT in the urban areas of the three countries. Urban expansion slightly reduces WBGT in the daytime, by 0.1–0.3°C, but substantially increases WBGT at night, by 0.5°C in India, and more than 1°C in China and Nigeria (Figure 3-a). Compared to India, the stronger nighttime urban warming in China and Nigeria is caused by the higher thermal conductivity of the building materials, which increases heat storage during daytime and releases more heat at night. Both urban heat island mitigation measures—installation of green and cool roofs—can reduce heat stress, although the latter is more effective than the former. The combination of urban land expansion and heat island mitigation leads to a total reduction in daytime WBGT by 1.2°C in China, and 0.6–0.7°C in India and Nigeria. At night, however, neither mitigation measures can fully counteract the heat stress increases from urban expansion; the net effect is an increase of 0.2–0.3°C in the nighttime WBGT in China and India and of ~0.9°C in Nigeria. If we restrict the analysis to urban areas in the arid regions, we find that urban land expansion has little effect on WBGT both during the daytime (<0.1°C) and nighttime (<0.3°C), and urban heat island mitigation measures are only half as effective as those in the humid regions (Figure 3-b).

The most severe increases in nighttime urban heat stress are concentrated in several population centers that already face substantial challenges in climate change adaptation. Although nighttime WBGT increases by less than 1°C in most urban areas from 2000 to 2050, the increase is much larger, by 2–3°C, in five hotspot mega-urban regions (MURs; Figure 4): A) Beijing-Tianjin-Hebei, located in the transition zone between cold and arid climates of northern China; B) Yangtze-River-Delta, in the temperate climate of eastern China, in the lower reaches of Yangtze River; C) Chengdu-Chongqing, in the temperate climate of southern China, in the middle reaches of Yangtze River; D) Delhi Metropolitan Area, in the transition zone between arid and temperate climates of northwestern India; and E) Port Harcourt, in the tropical coast of southern Nigeria. Even if cool roofs are installed, 1–1.5°C nighttime warming will remain in Yangtze-River Delta, Chengdu-Chongqing, and Delhi Metropolitan Area, and up to 2°C in Beijing-Tianjin-Hebei and Port Harcourt.

Owing to their various geographic conditions, these hotspot MURs will face different challenges in coping with the increasing urban heat stress. Beijing-Tianjin-Hebei and Delhi Metropolitan Area, two MURs located in the transition zones toward arid climates, face more severe water shortage due to accelerated dryland expansion (J. Huang et al., 2016) and depleted groundwater (J. Chen et al., 2014; Feng et al., 2013). Although the water-demanding green roofs are less effective as shown here, water resources are still needed to support street trees, which can mitigate heat stress by providing shade (Coutts et al., 2016)—a cooling strategy that is not included in our analysis. In Beijing-Tianjin-Hebei, the more effective cool roofs installment can lead to lower temperature in winter, increasing the cold-related health risks (Gasparrini et al., 2015) and building energy consumption (J. Yang, Wang, & Kaloush, 2015). The other three MURs (Yangtze-River Delta, Chengdu-Chongqing and Port Harcourt) rarely have water shortages or cold winters, but will experience more extreme heat events due to GHG-induced climate change. Annual heatwave days in the middle and lower reaches of Yangtze River, which includes Yangtze-River Delta and Chengdu-Chongqing, will increase from less than 10 now to ~80 by the end of 21st century, under the RCP8.5 scenario (Guo et al., 2017). Under this high emission scenario, heat stressed days in western Africa, which includes the Port Harcourt MUR, will increase from ~50 now to ~200 by the 2090s (Rohat et al., 2019). The persistent increases in nighttime urban heat stress shown here will likely further exacerbate the heat-related risks in these three MURs. Since previous studies showed that socioeconomic factors also affect residents' vulnerabilities to heat risks (Hu et al., 2017, 2019), we further distinguish the heat stress-related challenges in these MURs by comparing their income-levels by 2050. Table 2 shows the average GDP per capita by 2050 in the five MURs, calculated from the spatially gridded forecasts of population and GDP by (Murakami & Yamagata, 2019) (Figure S3). With GDP per capita higher than 30,000 (USD 2005), urban residents in the three MURs in China are less vulnerable to increasing heat stress. With GDP per capita of ~15,000 in Delhi Metropolitan Area and ~10,000 in Port Harcourt, urban residents in these two MURs will have higher challenges in heat stress adaptations. In these two MURs, government assistance in mitigating urban heat and providing heat shelters will be more critical. Moreover, given that cool roofs are less expensive than green roofs to install (Estrada et al., 2017), this adaptation should be given higher priority for the low-income households in these two MURs. Although green roofs are less effective in mitigating heat stress and are more expensive, they can provide ecological benefits (Williams et al., 2014) that may be needed in Port Harcourt, whose future expansion will threaten the biodiversity hotspot of Western African Forests (Myers et al., 2000; Seto et al., 2012).

To illuminate the mechanisms of the diurnally differentiated results shown above, Figure 5 disentangles the effects of urban land expansion (a–b) and heat island mitigation (c–d) on air temperature (x-axis) and relative humidity (y-axis), under the future climate conditions (2049–2055, RCP8.5). In these plots, each arrow indicates the mean change from 2000 to 2050 of urban areas located in a Köppen climate zone, and dashed lines are contours of WBGT. Urban land expansion raises daytime air temperature but reduces relative humidity in all climate zones except for arid hot desert climate (BWh), as indicated by the arrows pointing toward the lower-right directions (Figure 5-a). The arrows in the temperature-humidity-plane are mostly parallel to the contour lines of WBGT, meaning that the drying effects of urban expansion largely offset its warming effects and the result is little change in the daytime WBGT. During nighttime (Figure 5-b), however, most arrows cross the contour lines to the right, or in other words warming overwhelms drying, which results in WBGT increases. This diurnal asymmetry in heat stress changes is mainly due to the diurnally asymmetric effects of urban expansion on warming and drying. Table 1 shows that, in most climate zones, urban expansion raises air temperature more during nighttime than daytime, but it reduces specific humidity more during daytime than nighttime. The nighttime increase in air temperature is stronger because the replacement of rural landscape with urban area shifts daytime sensible and latent heat fluxes to heat storage, which is released at nighttime. The daytime decrease in specific humidity is stronger because the replacement of vegetated landscape with impervious urban area significantly reduces ET during daytime; whereas at night, the drying effect is weaker since there is little ET to be reduced.

Urban heat island mitigation measures (Figure 5 c & d) reduce air temperature but increase humidity, which is not surprising for green roof installment whose evaporative cooling adds extra moisture into the atmosphere. What may seem counterintuitive is that cool roof installment, which reduces surface solar radiation absorption by increasing albedo, also raises humidity. This drying effect of cool roofs can be explained by the evolution of atmospheric boundary layer (ABL) (X. Lee, 2018). In this cool-roof scenario, less solar radiation energy is available to drive convection and as a result the ABL is shallower (Epstein et al., 2017), concentrating in a smaller volume the water vapor that originates at the ground, thereby increasing humidity.

To determine whether the diurnal and geographic variations presented above will be affected by global climate change, we repeat the model calculation with two sets of boundary conditions (invariant urban areas versus urban expansion scenario) and two GHG scenarios (one in current climate and another in future climate under RCP 8.5), for a total of four permutations. Figure S1 shows the changes in WBGT due to urban expansion under current (1999–2004; y-axis) and future (2049–2054, RCP 8.5; x-axis) climate conditions. Under both climate conditions, urban expansion results in daytime cooling (left panel) and nighttime warming (right panel) for 68.2% and 70.5% of urban areas in 2050, respectively. Across geographic locations, WBGT changes under the two climate conditions are strongly correlated ($R^2 = 0.85$ in daytime and 0.91 in nighttime). These results suggest that nonlinear interactions between urban expansion and GHG emission are nearly negligible and that the overall effect can be estimated by linearly adding the effects from urban expansion and the effects from GHG emission. These results may seem contradictory to a recent study that showed nonlinear interactive effects on surface air temperature between urban expansion and GHG emission (Krayenhoff et al., 2018). This apparent contradiction arises mostly from the fact that the WBGT change has accounted for both temperature change and humidity change. The interaction between GHG emission and urban expansion can be defined as the difference of urban expansion-induced changes under future and current climate conditions. We quantified the interactive effects on air temperature (T_a), relative humidity (RH), and WBGT, during the daytime (Table S1) and nighttime (Table S2), in seven climate zones where the majority of future urban areas will be located. The interactive effects on T_a and RH are the opposite, resulting in little change in WBGT, in urban areas in the tropical savannah (Aw), arid (BSh & BSk), humid subtropical (Cwa) and continental (Dwb) climates, accounting for about 76% of all urban areas in 2050 of our study regions. Our analysis suggests that, for a large portion of future urban areas, it is possible to superimpose the effects on heat stress from urbane expansion presented here on those from climate change under other GHG scenarios, when projecting future heat stress on urban residents.

4 Discussions

Using atmospheric modeling and urban expansion projections and by combining air temperature and humidity predictions, we reveal a diurnal pattern of future urban heat stress that has been missing in existing literature. Our results show that urban expansion increases heat stress (quantified as modified WBGT in this paper) much more at night than during the day. Our results also show that urban heat island mitigation measures have the potential to reduce daytime heat stress but bring little change to nighttime stress (Figure 3).

Increasing urban heat stress can amplify health risks and energy consumptions. The persistent nighttime urban warming revealed herein suggests heat mitigation measures need to prioritize residential buildings, where most urban dwellers spend the night. There is evidence that, compared to daytime, exposure to nighttime extreme heat contributes more to mortality risks, especially in urban areas (Laaidi et al., 2011; Murage et al., 2017). In less extreme conditions, hotter nights nevertheless still disrupt sleep patterns (Obradovich et al., 2017), leading to physiological and psychological harms. While most of the heat-health effects studies are based on only air temperature, there is emerging empirical evidence (Heo et al., 2019; Heo & Bell, 2018) showing that heat stress indices that account for humidity can better explain the health outcomes. However, these heat-related health impact studies focus either on nighttime air temperature or daytime heat stress, providing limited understanding on the quantitative relationship between nighttime heat stress and health. Further studies on the health impacts of nighttime heat stress are needed, in the manner of this study, in order to better understand how urban expansion might threaten human health.

One of the most effective ways to reduce heat stress is by cooling indoor spaces. However, according to a recent projection by International Energy Agency (IEA, 2018) that includes both temperature and humidity, energy demands for indoor cooling will increase threefold from 2,020 terawatt-hours (TWh) in 2016 to 6,200 TWh in 2050, accounting for 30% of the global building electricity use. This IEA projection incorporates future population and economic growth, and a 1°C GHG-induced global warming, but ignores the warming caused by urban expansion. Without considering urban expansion-warming, it is projected that about 70% of the increase in global cooling energy use will come from the residential sector, and that China and India will account for more than half of the global expansion in the capacity of residential indoor cooling. The urban expansion-induced nighttime WBGT increases associated with urban expansion showed here imply an underestimation in the IEA cooling energy use projection that only considers GHG emissions. Since most urban residents spend the nights at home, our results expansion-induced nighttime warming of WBGT in China and India indicate that future cooling energy use will be substantially higher than the existing projection. According to the assumption that a 1°C warming corresponds to 25% increase in cooling loads used in the IEA projection, our result of ~1°C nighttime WBGT warming in China and India suggests that the energy used for cooling their cities at night will probably be higher by about a quarter. Since indoor cooling also intensifies UHI by releasing waste heat, future modeling research accounting for the interactions between heat stress, urban expansion, and indoor cooling is still needed to reliably quantify future urban expansion's impact on energy use.

The potential impacts on human health and energy use discussed above demonstrate the needs to mitigate future increase in nighttime heat stress caused by urban expansion. However, our results show that infrastructure-based urban heat island (UHI) mitigation measures—installing green/cool roofs—can increase relative humidity via increasing surface evaporation (green roofs) or suppressing the atmospheric boundary layer (cool roofs), making those forms of mitigation less effective in reducing WBGT (Figure 3 and Figure 5). Our analysis suggests that even if green/cool roofs are deployed at a large-scale, these UHI mitigation measures can only reduce about half of the urban expansion-induced increase in nighttime heat stress. Mitigating the persistent nighttime heat stress in the rapidly expanding Asian and African cities will require multi-disciplinary solutions beyond the green/cool roofs often examined in atmospheric studies (Georgescu et al., 2014; Stone et al., 2014; Zhao et al., 2017). One possible complementary strategy against nighttime urban heat stress is improving insulation of residential buildings. Since cool roofs have been shown to reduce indoor heat stress by 26–46% (Zinzi & Agnoli, 2012), improved building insulation can prevent the persistent half of outdoor WBGT increase from compromising indoor thermal comfort. Because the ~0.4 million km^2 of future urban areas in China, India and Nigeria do not exist now and will be built in the next decades (K. Huang et al., 2019), establishing regulations on cool roofs and residential building insulation can generate potential benefits of heat stress mitigation for ~8 million additional urban residents in these countries by 2050 (UN DESA, 2014).

Our results show that the combination of urban land expansion and heat island mitigation has the potential during daytime to reduce heat stress, providing an opportunity to delay un-inhabitable climate conditions. Due to global climate change under the RCP 8.5 scenario, by the end of 21st century, daily maximum heat stress in northeastern South Asia and eastern China will approach or exceed the critical threshold of 35°C wet-bulb temperature, beyond which human bodies cannot sufficiently cool off by sweating (Im et al., 2017; Kang & Eltahir, 2018). Because extreme heat stress usually occurs in the afternoon (C. Raymond et al., 2017), our results regarding daytime urban cooling, suggest that urban expansion by 2050, with cool roofs installed, can potentially delay the exceedance of critical heat stress thresholds, allowing extra time for GHG emission mitigation or strategic retreat from those un-inhabitable regions. However, since observed heat stress extremes are mainly driven by horizontal transport of moisture (C. Raymond et al., 2017; Colin Raymond et al., 2020), it is unclear whether the local drying effects of urban expansion are strong enough to counteract moisture advection. Further modeling studies to investigate the interaction between urban expansion and moisture transport are still needed to understand the potential benefits of avoiding exceedance of heat stress thresholds. In less extreme conditions, WBGT higher than 25°C, albeit not lethal, can lead to labor capacity loss in outdoor environments. Even if GHG-induced global warming is limited to a 2°C change from pre-industrial level, global labor capacity loss, especially in low- to mid-latitudes, will more than double from 10% now to 25% by 2050 due to rising heat stress (Dunne et al., 2013). Our result of ~1°C reduction in daytime WBGT from combining urban expansion and adaptation shows the potential to alleviate labor productivity loss in urban areas. Improving outdoor labor productivity will be critical in maintaining the gray urban infrastructures, such as pavements and power supplies, whose degradation has been projected to accelerate with global climate change (Forzieri et al., 2018; Underwood et al., 2017).

One important caveat of our analysis is the inadequate representation of shade and wind in our quantification of heat stress and atmospheric modeling. In addition to air temperature and humidity, thermal comfort is also affected by the direct solar radiation on human bodies, which can be reduced by shading (Harlan et al., 2006). Our analysis cannot adequately address the shading effects for two reasons. First, shading depends on various urban form factors, such as building heights, street widths, and tree canyons. Accounting for variations in urban forms requires analyses that are beyond the scope of this paper—the effects of adding new urban areas with similar structures to the existing ones. Second, the tree-canopy representation in the WRF model does not adequately capture the cooling effects from shading (Wang et al., 2016). To address this caveat, multiple scenarios of various urban forms and an improved urban-canyon-tree-canopy model need to be included in future studies. Nonetheless, considering the shading effects, it is reasonable to speculate that urban forms with narrower streets and more street trees have the potential to further reduce daytime heat stress.

5 Conclusions

The climate is changing and the world is urbanizing rapidly. Both processes can potentially increase heat stress in urban areas, yet the effects of urban expansion remain unclear. Our results, from simulating the effects of urban expansion on both temperature and humidity, reveal a new diurnal pattern of changing heat stress. During daytime conditions, urban land expansion and heat island mitigation provide the opportunity to delay extreme heat conditions caused by climate change. During nighttime conditions, the persistent warming at night can exacerbate increases in health risks and energy consumption, which requires complementary measures like combining green/cool roofs with improved building insulation.

Acknowledgements

This research was supported by the NSAS Earth and Space Science Fellowship (NESSF) Program (grant 80NSSC17K00447), the Yale Institute of Biospheric Studies, the Yale Hixon Center for Urban Ecology, the Yale Tropical Resources Institute, and a Yale University Graduate Fellowship. X Lee acknowledges support by the US National Science Foundation (grant AGS1933630).

Data Availability Statement

The results of nighttime WBGT increases are available for download at figshare (https://figshare.com/s/9b991f83366a29c45e09 and https://figshare.com/s/0d61755f759d40d5bc6f). Full WRF outputs are not deposited on public data repository due to the large file sizes. These outputs are available upon request from the correspondence author K. Huang. Other data needed to run the simulations include: the spatially explicit, probabilistic forecasts of global urban land expansion by 2050 (https://doi.org/10.6084/m9.figshare.7897010) and the NCAR CESM Global Bias-Corrected CMIP5 Output to Support WRF/MPAS Research (https://rda.ucar.edu/datasets/ds316.1/).

References

Ackerman, B. (1987). Climatology of Chicago Area Urban-Rural Differences in Humidity. *Journal of Climate and Applied Meteorology*, *26*(3), 427–430. https://doi.org/10.1175/1520-0450(1987)026<0427:COCAUR>2.0.CO;2

Adebayo, Y. R. (1991). Day-time effects of urbanization on relative humidity and vapour pressure in a tropical city. *Theoretical and Applied Climatology*, *43*(1–2), 17–30. https://doi.org/10.1007/BF00865039

Ahmadalipour, A., & Moradkhani, H. (2018). Escalating heat-stress mortality risk due to global warming in the Middle East and North Africa (MENA). *Environment International*, *117*, 215–225. https://doi.org/10.1016/j.envint.2018.05.014

d'Ambrosio Alfano, F. R., Malchaire, J., Palella, B. I., & Riccio, G. (2014). WBGT Index Revisited After 60 Years of Use. *The Annals of Occupational Hygiene*, *58*(8), 955–970. https://doi.org/10.1093/annhyg/meu050

Beck, H. E., Zimmermann, N. E., McVicar, T. R., Vergopolan, N., Berg, A., & Wood, E. F. (2018). Present and future Köppen-Geiger climate classification maps at 1-km resolution. *Scientific Data*, *5*, 180214. https://doi.org/10.1038/sdata.2018.214

Blazejczyk, K., Epstein, Y., Jendritzky, G., Staiger, H., & Tinz, B. (2012). Comparison of UTCI to selected thermal indices. *International Journal of Biometeorology*, *56*(3), 515–535. https://doi.org/10.1007/s00484-011-0453-2

Brocherie, F., & Millet, G. P. (2015). Is the Wet-Bulb Globe Temperature (WBGT) Index Relevant for Exercise in the Heat? *Sports Medicine*, *45*(11), 1619–1621. https://doi.org/10.1007/s40279-015-0386-8

Bruyere, L., Monaghan, J., Steinhoff, F., & Yates, D. (2015). Bias-Corrected CMIP5 CESM Data in WRF/MPAS Intermediate File Format. https://doi.org/10.5065/D6445JJ7

Chen, F., Yang, X., & Wu, J. (2016). Simulation of the urban climate in a Chinese megacity with spatially heterogeneous anthropogenic heat data. *Journal of Geophysical Research: Atmospheres*, *121*(10), 5193–5212. https://doi.org/10.1002/2015JD024642

Chen, J., Li, J., Zhang, Z., & Ni, S. (2014). Long-term groundwater variations in Northwest India from satellite gravity measurements. *Global and Planetary Change*, *116*, 130–138. https://doi.org/10.1016/j.gloplacha.2014.02.007

Chen, L., & Frauenfeld, O. W. (2016). Impacts of urbanization on future climate in China. *Climate Dynamics*, *47*(1–2), 345–357. https://doi.org/10.1007/s00382-015-2840-6

Coutts, A. M., White, E. C., Tapper, N. J., Beringer, J., & Livesley, S. J. (2016). Temperature and human thermal comfort effects of street trees across three contrasting street canyon environments. *Theoretical and Applied Climatology*, *124*(1), 55–68. https://doi.org/10.1007/s00704-015-1409-y

Dunne, J. P., Stouffer, R. J., & John, J. G. (2013). Reductions in labour capacity from heat stress under climate warming. *Nature Climate Change*, *3*(6), 563–566. https://doi.org/10.1038/nclimate1827

Epstein, S. A., Lee, S.-M., Katzenstein, A. S., Carreras-Sospedra, M., Zhang, X., Farina, S. C., et al. (2017). Air-quality implications of widespread adoption of cool roofs on ozone and particulate matter in southern California. *Proceedings of the National Academy of Sciences*, *114*(34), 8991–8996. https://doi.org/10.1073/pnas.1703560114

Estrada, F., Botzen, W. J. W., & Tol, R. S. J. (2017). A global economic assessment of city policies to reduce climate change impacts. *Nature Climate Change*, *7*(6), 403–406. https://doi.org/10.1038/nclimate3301

Feng, W., Zhong, M., Lemoine, J.-M., Biancale, R., Hsu, H.-T., & Xia, J. (2013). Evaluation of groundwater depletion in North China using the Gravity Recovery and Climate Experiment (GRACE) data and ground-based measurements. *Water Resources Research*, *49*(4), 2110–2118. https://doi.org/10.1002/wrcr.20192

Fischer, E. M., & Knutti, R. (2013). Robust projections of combined humidity and temperature extremes. *Nature Climate Change*, *3*(2), 126–130. https://doi.org/10.1038/nclimate1682

Forzieri, G., Bianchi, A., Silva, F. B. e, Marin Herrera, M. A., Leblois, A., Lavalle, C., et al. (2018). Escalating impacts of climate extremes on critical infrastructures in Europe. *Global Environmental Change*, *48*, 97–107. https://doi.org/10.1016/j.gloenvcha.2017.11.007

Gasparrini, A., Guo, Y., Hashizume, M., Lavigne, E., Zanobetti, A., Schwartz, J., et al. (2015). Mortality risk attributable to high and low ambient temperature: a multicountry observational study. *The Lancet*, *386*(9991), 369–375. https://doi.org/10.1016/S0140-6736(14)62114-0

Georgescu, M., Morefield, P. E., Bierwagen, B. G., & Weaver, C. P. (2014). Urban adaptation can roll back warming of emerging megapolitan regions. *Proceedings of the National Academy of Sciences*, *111*(8), 2909–2914. https://doi.org/10.1073/pnas.1322280111

Guo, X., Huang, J., Luo, Y., Zhao, Z., & Xu, Y. (2017). Projection of heat waves over China for eight different global warming targets using 12 CMIP5 models. *Theoretical and Applied Climatology*, *128*(3), 507–522. https://doi.org/10.1007/s00704-015-1718-1

Harlan, S. L., Brazel, A. J., Prashad, L., Stefanov, W. L., & Larsen, L. (2006). Neighborhood microclimates and vulnerability to heat stress. *Social Science & Medicine*, *63*(11), 2847–2863. https://doi.org/10.1016/j.socscimed.2006.07.030

Heo, S., & Bell, M. L. (2018). Heat waves in South Korea: differences of heat wave characteristics by thermal indices. *Journal of Exposure Science & Environmental Epidemiology*, 1–16. https://doi.org/10.1038/s41370-018-0076-3

Heo, S., Bell, M. L., & Lee, J.-T. (2019). Comparison of health risks by heat wave definition: Applicability of wet-bulb globe temperature for heat wave criteria. *Environmental Research*, *168*, 158–170. https://doi.org/10.1016/j.envres.2018.09.032

Hu, K., Yang, X., Zhong, J., Fei, F., & Qi, J. (2017). Spatially Explicit Mapping of Heat Health Risk Utilizing Environmental and Socioeconomic Data. *Environmental Science & Technology*, *51*(3), 1498–1507. https://doi.org/10.1021/acs.est.6b04355

Hu, K., Guo, Y., Hochrainer-Stigler, S., Liu, W., See, L., Yang, X., et al. (2019). Evidence for Urban-Rural Disparity in Temperature-Mortality Relationships in Zhejiang Province, China. *Environmental Health Perspectives*, *127*(3), 37001. https://doi.org/10.1289/EHP3556

Huang, J., Yu, H., Guan, X., Wang, G., & Guo, R. (2016). Accelerated dryland expansion under climate change. *Nature Climate Change*, *6*(2), 166–171. https://doi.org/10.1038/nclimate2837

Huang, K., Li, X., Liu, X., & Seto, K. C. (2019). Projecting global urban land expansion and heat island intensification through 2050. *Environmental Research Letters*, *14*(11), 114037. https://doi.org/10.1088/1748-9326/ab4b71

IEA. (2018). *The Future of Cooling: Opportunities for energy-efficient air conditioning*. International Energy Agency. Retrieved from https://webstore.iea.org/the-future-of-cooling

Im, E.-S., Pal, J. S., & Eltahir, E. A. B. (2017). Deadly heat waves projected in the densely populated agricultural regions of South Asia. *Science Advances*, *3*(8), e1603322. https://doi.org/10.1126/sciadv.1603322

Jackson, T. L., Feddema, J. J., Oleson, K. W., Bonan, G. B., & Bauer, J. T. (2010). Parameterization of Urban Characteristics for Global Climate Modeling. *Annals of the Association of American Geographers*, *100*(4), 848–865. https://doi.org/10.1080/00045608.2010.497328

Kang, S., & Eltahir, E. A. B. (2018). North China Plain threatened by deadly heatwaves due to climate change and irrigation. *Nature Communications*, *9*(1), 1–9. https://doi.org/10.1038/s41467-018-05252-y

Knauer, J., El-Madany, T. S., Zaehle, S., & Migliavacca, M. (2018). Bigleaf—An R package for the calculation of physical and physiological ecosystem properties from eddy covariance data. *PLOS ONE*, *13*(8), e0201114. https://doi.org/10.1371/journal.pone.0201114

Krayenhoff, E. S., Moustaoui, M., Broadbent, A. M., Gupta, V., & Georgescu, M. (2018). Diurnal interaction between urban expansion, climate change and adaptation in US cities. *Nature Climate Change*, *8*(12), 1097. https://doi.org/10.1038/s41558-018-0320-9

Laaidi, K., Zeghnoun, A., Dousset, B., Bretin, P., Vandentorren, S., Giraudet, E., & Beaudeau, P. (2011). The Impact of Heat Islands on Mortality in Paris during the August 2003 Heat Wave. *Environmental Health Perspectives*, *120*(2), 254–259. https://doi.org/10.1289/ehp.1103532

Lee, D. O. (1991). Urban—rural humidity differences in London. *International Journal of Climatology*, *11*(5), 577–582. https://doi.org/10.1002/joc.3370110509

Lee, X. (2018). *Fundamentals of Boundary-Layer Meteorology*. Springer International Publishing. Retrieved from https://www.springer.com/gp/book/9783319608518

Li, D., Bou-Zeid, E., & Oppenheimer, M. (2014). The effectiveness of cool and green roofs as urban heat island mitigation strategies. *Environmental Research Letters*, *9*(5), 055002. https://doi.org/10.1088/1748-9326/9/5/055002

Li, J., Chen, Y. D., Gan, T. Y., & Lau, N.-C. (2018). Elevated increases in human-perceived temperature under climate warming. *Nature Climate Change*, *8*(1), 43–47. https://doi.org/10.1038/s41558-017-0036-2

Lucas, R. A. I., Epstein, Y., & Kjellstrom, T. (2014). Excessive occupational heat exposure: a significant ergonomic challenge and health risk for current and future workers. *Extreme Physiology & Medicine*, *3*(1), 14. https://doi.org/10.1186/2046-7648-3-14

Luo, M., & Lau, N.-C. (2019). Urban Expansion and Drying Climate in an Urban Agglomeration of East China. *Geophysical Research Letters*, *46*(12), 6868–6877. https://doi.org/10.1029/2019GL082736

Matthews, T. K. R., Wilby, R. L., & Murphy, C. (2017). Communicating the deadly consequences of global warming for human heat stress. *Proceedings of the National Academy of Sciences*, *114*(15), 3861–3866. https://doi.org/10.1073/pnas.1617526114

Miao, S., & Chen, F. (2014). Enhanced modeling of latent heat flux from urban surfaces in the Noah/single-layer urban canopy coupled model. *Science China Earth Sciences*, *57*(10), 2408–2416. https://doi.org/10.1007/s11430-014-4829-0

Monteith, J., & Unsworth, M. (2013). *Principles of Environmental Physics: Plants, Animals, and the Atmosphere* (4 edition). Academic Press.

Murage, P., Hajat, S., & Kovats, R. S. (2017). Effect of night-time temperatures on cause and age-specific mortality in London. *Environmental Epidemiology*, *1*(2), e005. https://doi.org/10.1097/EE9.0000000000000005

Murakami, D., & Yamagata, Y. (2019). Estimation of Gridded Population and GDP Scenarios with Spatially Explicit Statistical Downscaling. *Sustainability*, *11*(7), 2106. https://doi.org/10.3390/su11072106

Myers, N., Mittermeier, R. A., Mittermeier, C. G., da Fonseca, G. A. B., & Kent, J. (2000). Biodiversity hotspots for conservation priorities. *Nature*, *403*(6772), 853–858. https://doi.org/10.1038/35002501

Obradovich, N., Migliorini, R., Mednick, S. C., & Fowler, J. H. (2017). Nighttime temperature and human sleep loss in a changing climate. *Science Advances*, *3*(5), e1601555. https://doi.org/10.1126/sciadv.1601555

Oke, T. R. (1982). The energetic basis of the urban heat island. *Quarterly Journal of the Royal Meteorological Society*, *108*(455), 1–24. https://doi.org/10.1002/qj.49710845502

Pal, J. S., & Eltahir, E. A. B. (2016). Future temperature in southwest Asia projected to exceed a threshold for human adaptability. *Nature Climate Change*, *6*(2), 197–200. https://doi.org/10.1038/nclimate2833

Patel, T., Mullen, S. P., & Santee, W. R. (2013). Comparison of Methods for Estimating Wet-Bulb Globe Temperature Index From Standard Meteorological Measurements. *Military Medicine*, *178*(8), 926–933. https://doi.org/10.7205/MILMED-D-13-00117

Raymond, C., Singh, D., & Horton, R. M. (2017). Spatiotemporal Patterns and Synoptics of Extreme Wet-Bulb Temperature in the Contiguous United States. *Journal of Geophysical Research: Atmospheres*, *122*(24), 13,108-13,124. https://doi.org/10.1002/2017JD027140

Raymond, Colin, Matthews, T., & Horton, R. M. (2020). The emergence of heat and humidity too severe for human tolerance. *Science Advances*, *6*(19), eaaw1838. https://doi.org/10.1126/sciadv.aaw1838

Rohat, G., Flacke, J., Dosio, A., Dao, H., & Maarseveen, M. van. (2019). Projections of Human Exposure to Dangerous Heat in African Cities Under Multiple Socioeconomic and Climate Scenarios. *Earth's Future*, *7*(5), 528–546. https://doi.org/10.1029/2018EF001020

Seto, K. C., Güneralp, B., & Hutyra, L. R. (2012). Global forecasts of urban expansion to 2030 and direct impacts on biodiversity and carbon pools. *Proceedings of the National Academy of Sciences*, *109*(40), 16083–16088. https://doi.org/10.1073/pnas.1211658109

Sherwood, S. C., & Huber, M. (2010). An adaptability limit to climate change due to heat stress. *Proceedings of the National Academy of Sciences*, *107*(21), 9552–9555. https://doi.org/10.1073/pnas.0913352107

Skamarock, C., Klemp, B., Dudhia, J., Gill, O., Barker, D., Duda, G., et al. (2008). A Description of the Advanced Research WRF Version 3. https://doi.org/10.5065/D68S4MVH

Smith, A., Lott, N., & Vose, R. (2011). The Integrated Surface Database: Recent Developments and Partnerships. *Bulletin of the American Meteorological Society*, *92*(6), 704–708. https://doi.org/10.1175/2011BAMS3015.1

Stone, B. (2012). *The City and the Coming Climate: Climate Change in the Places We Live* (1 edition). New York: Cambridge University Press.

Stone, B., Vargo, J., Liu, P., Habeeb, D., DeLucia, A., Trail, M., et al. (2014). Avoided Heat-Related Mortality through Climate Adaptation Strategies in Three US Cities. *PLoS ONE*, *9*(6), e100852. https://doi.org/10.1371/journal.pone.0100852

Um, H.-H., Ha, K.-J., & Lee, S.-S. (2007). Evaluation of the urban effect of long-term relative humidity and the separation of temperature and water vapor effects. *International Journal of Climatology*, *27*(11), 1531–1542. https://doi.org/10.1002/joc.1483

UN DESA. (2014). *World Urbanization Prospects: The 2014 Revision, Highlights*. New York: United Nations, Department of Economic and Social Affairs, Population Division. Retrieved from http://esa.un.org/unpd/wup/highlights/wup2014-highlights.pdf

Underwood, B. S., Guido, Z., Gudipudi, P., & Feinberg, Y. (2017). Increased costs to US pavement infrastructure from future temperature rise. *Nature Climate Change*, *7*(10), 704–707. https://doi.org/10.1038/nclimate3390

Vuuren, D. P. van, Edmonds, J., Kainuma, M., Riahi, K., Thomson, A., Hibbard, K., et al. (2011). The representative concentration pathways: an overview. *Climatic Change*, *109*(1–2), 5–31. https://doi.org/10.1007/s10584-011-0148-z

Wang, Z.-H., Zhao, X., Yang, J., & Song, J. (2016). Cooling and energy saving potentials of shade trees and urban lawns in a desert city. *Applied Energy*, *161*, 437–444. https://doi.org/10.1016/j.apenergy.2015.10.047

Williams, N. S. G., Lundholm, J., & MacIvor, J. S. (2014). FORUM: Do green roofs help urban biodiversity conservation? *Journal of Applied Ecology*, *51*(6), 1643–1649. https://doi.org/10.1111/1365-2664.12333

Yang, B., Yang, X., Leung, L. R., Zhong, S., Qian, Y., Zhao, C., et al. (2019). Modeling the Impacts of Urbanization on Summer Thermal Comfort: The Role of Urban Land Use and Anthropogenic Heat. *Journal of Geophysical Research: Atmospheres*, *124*(13), 6681–6697. https://doi.org/10.1029/2018JD029829

Yang, J., Wang, Z.-H., Chen, F., Miao, S., Tewari, M., Voogt, J. A., & Myint, S. (2015). Enhancing Hydrologic Modelling in the Coupled Weather Research and Forecasting–Urban Modelling System. *Boundary-Layer Meteorology*, *155*(1), 87–109. https://doi.org/10.1007/s10546-014-9991-6

Yang, J., Wang, Z.-H., & Kaloush, K. E. (2015). Environmental impacts of reflective materials: Is high albedo a 'silver bullet' for mitigating urban heat island? *Renewable and Sustainable Energy Reviews*, *47*, 830–843. https://doi.org/10.1016/j.rser.2015.03.092

Zhao, L., Lee, X., & Schultz, N. M. (2017). A wedge strategy for mitigation of urban warming in future climate scenarios. *Atmospheric Chemistry and Physics*, *17*(14), 9067–9080. https://doi.org/10.5194/acp-17-9067-2017

Zinzi, M., & Agnoli, S. (2012). Cool and green roofs. An energy and comfort comparison between passive cooling and mitigation urban heat island techniques for residential buildings in the Mediterranean region. *Energy and Buildings*, *55*, 66–76. https://doi.org/10.1016/j.enbuild.2011.09.024

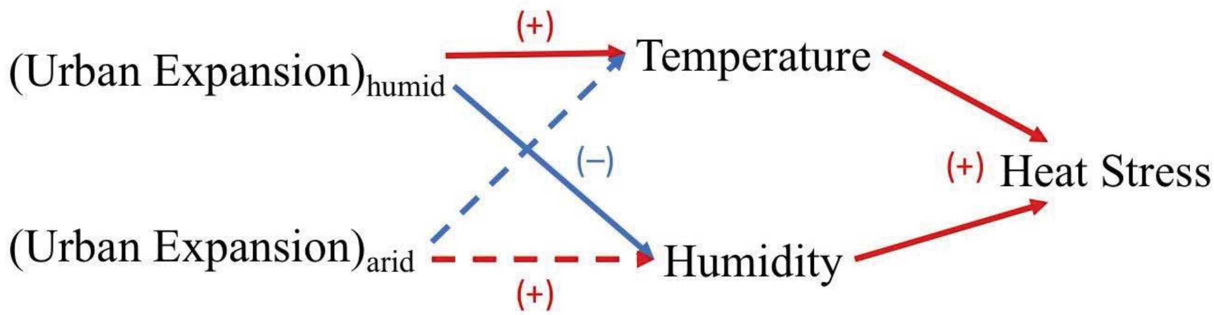

Figure 1 Mechanisms of urban expansion affecting heat stress, in humid and arid climates.

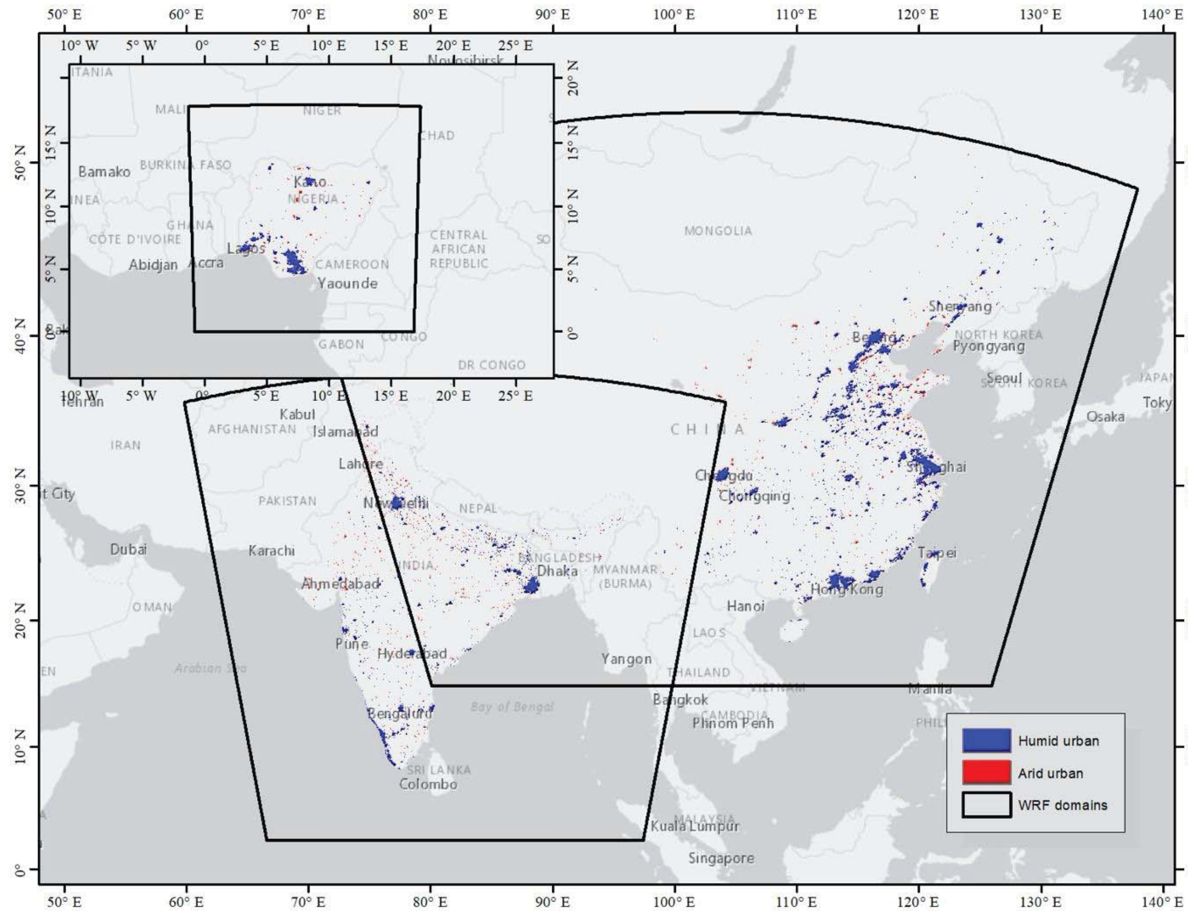

Figure 2 The domains for the Weather Research and Forecasting (WRF) simulations and the geographic distributions of humid and arid urban areas in China, India, and Nigeria.

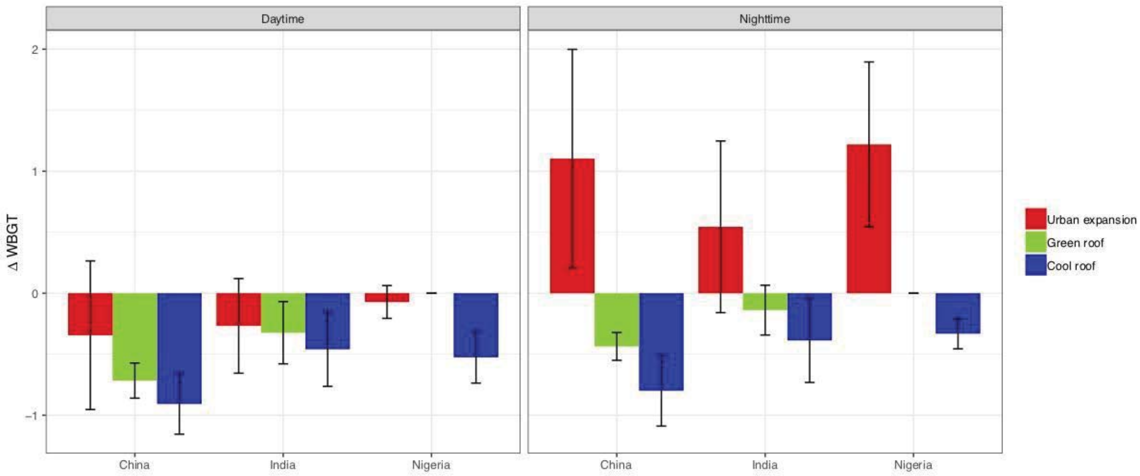

a

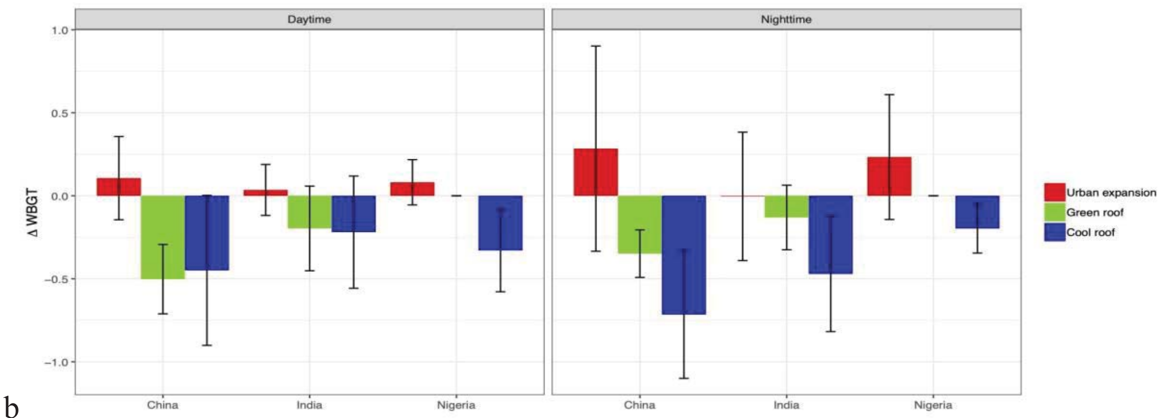

b

Figure 3 Summer average changes in wet-bulb globe temperature (WBGT) in humid (a) and arid (b) urban lands, due to urban land expansion and heat island mitigations. Urban heat island mitigation measures include installing green and cool roofs, and the changes are calculated using urban land expansion scenario as the baseline. Error bars represent one standard deviation from the regional means.

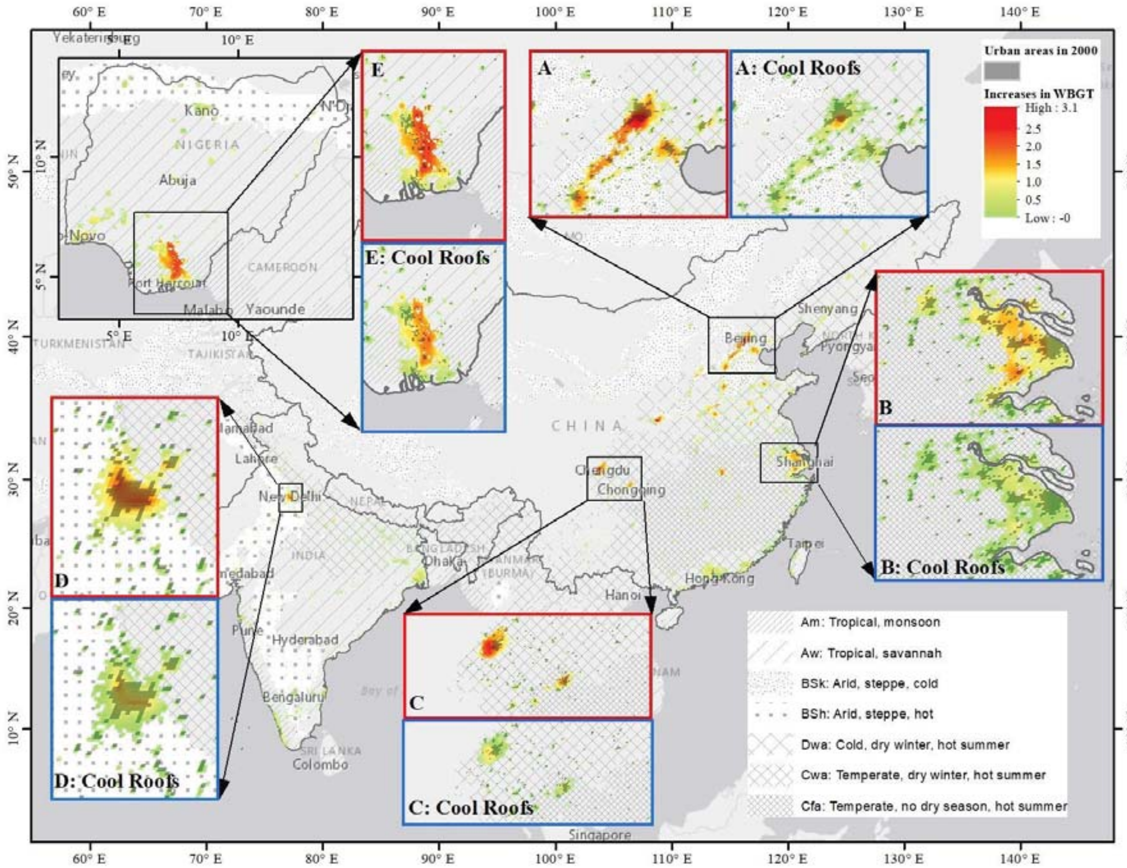

Figure 4 Geographic distributions of changes in nighttime wet-bulb globe temperature (WBGT) due to urban expansion. Enlarged maps with red frames show five mega urban regions with >2°C warming: A) Beijing-Tianjin-Hebei, B) Yangtze River Delta, C) Chengdu-Chongqing, D) Delhi Metropolitan Area, and E) Port Harcourt, and those with blue frames show the respective warming with installment of cool roofs. (Base map credits: ESRI, HERE, Garmin, © OpenStreetMap contributors, and the GIS user community.)

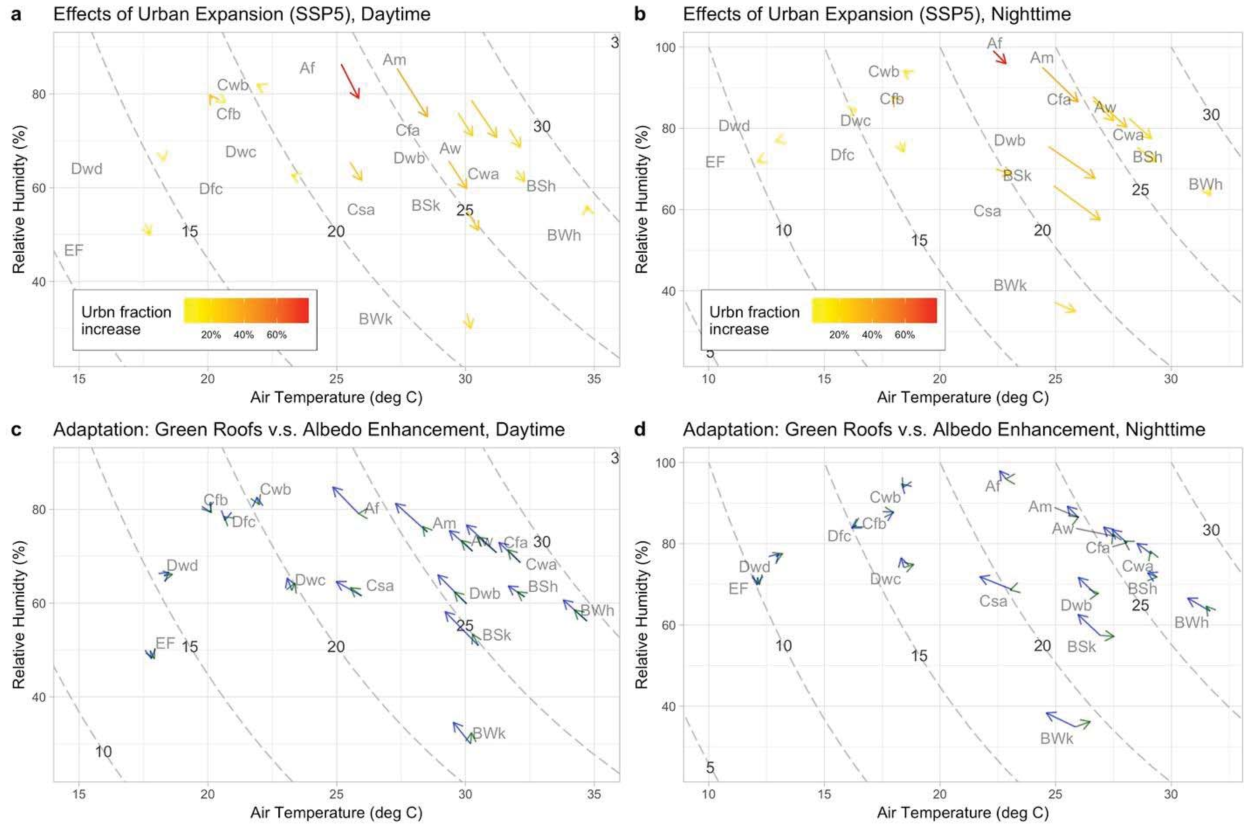

Figure 5 Effects of urban land expansion (a-b) and heat mitigation (c-d) on air temperature (x-axis), relative humidity (y-axis), and wet-bulb globe temperature (WBGT, black dashed curves), during daytime (a and c) and nighttime (b and d), in future climate conditions (2049–2054, RCP8.5). Arrows represent the average effects of urban grids within the same Köppen climate zones[49]: in a-b heads and tails are conditions of before and after land urban expansion, and in c-d heads and tails are without and with urban heat island mitigation measures. In c-d, green arrows represent the effects of installing green roofs and blue ones represent those of cool roofs. Köppen climates notations: A-tropical, B-arid, C-temperate, D-cold, W: desert, S: steppe, h: hot, k: cold, m-monsoon, w-dry winter, s-dry summer, f-no dry season, a-hot summer, b-warm summer, c-cold summer.

Table 1 Changes in air temperature and specific humidity due to urban expansion during daytime and nighttime, in different climate zones.

	Air temperature (°C)		Specific humidity (g/kg)		Percentage of total urban area in 2050
Climate zone	Daytime	Nighttime	Daytime	Nighttime	
Am: Tropical, monsoon	1.30	1.72	-1.25	0.00	7%
Aw: Tropical, savannah	0.58	0.91	-0.65	-0.12	23%
BSh: Arid, steppe, hot	0.33	0.87	-0.46	-0.08	8%
BSk: Arid, steppe, cold	0.47	2.13	-0.73	-0.04	5%
Cfa: Temperate, no dry season, hot summer	1.02	1.55	-1.08	-0.03	14%
Cwa: Temperate, dry winter, hot summer	0.45	1.02	-0.57	-0.06	26%
Dwb: Cold, dry winter, warm summer	0.76	2.15	-6.73	0.14	14%

Table 2 Average GDP per capita (PPP, USD 2005/year) in the five mega-urban regions (MURs).

MUR	GDP per capita (PPP, USD 2005)
Beijing-Tianjin-Hebei	33,024
Yangtze-River-Delta	42,843
Chengdu-Chongqing	31,592
Delhi Metropolitan Area	15,577
Port Harcourt	10,187

Figure 1.

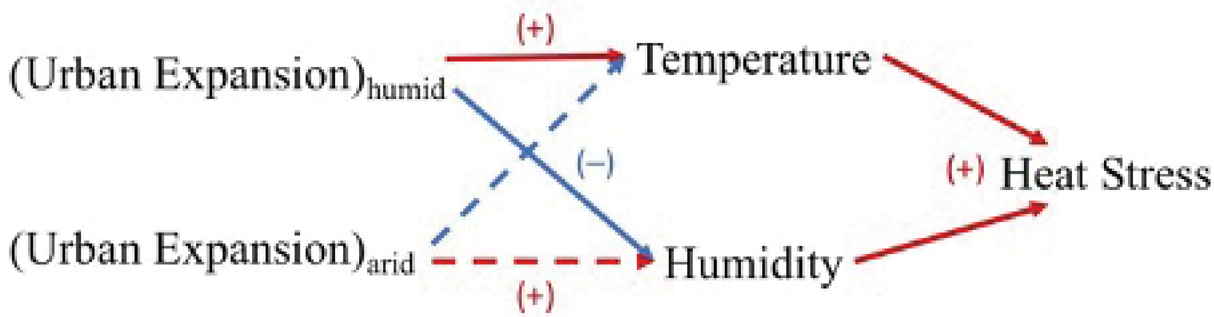
(+)
(Urban Expansion)humid
Temperature
(−)
(+) Heat Stress
(Urban Expansion)arid
Humidity
(+)

Figure 2.

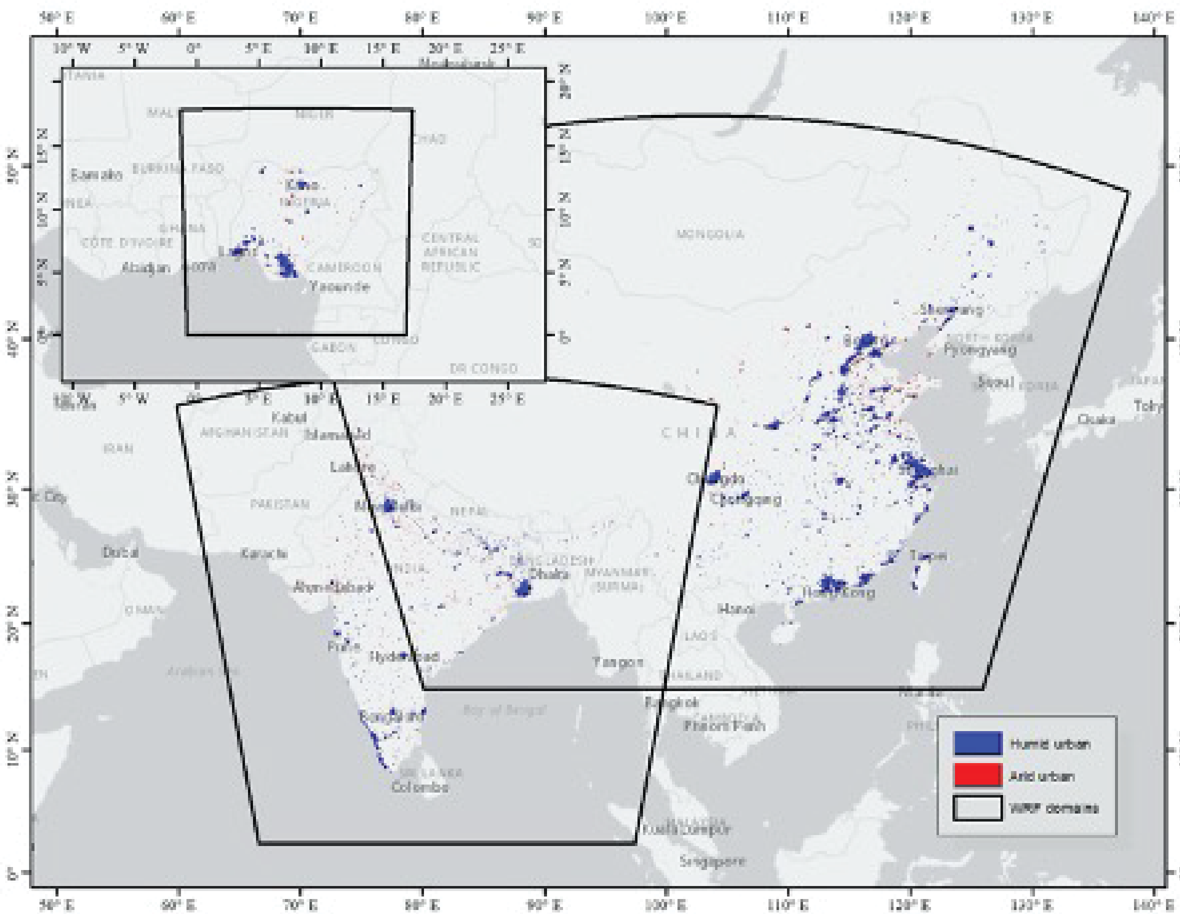

Humid urban
Arid urban
WRF domains
MONGOLIA
CHINA
Beijing
Shanghai
Hong Kong
Taipei
Seoul
Pyongyang
Shenyang
Osaka
Chengdu
Chongqing
Hanoi
Yangon
Bangkok
Phnom Penh
Kuala Lumpur
Singapore
Dhaka
Hyderabad
Colombo
Karachi
Lahore
Islamabad
Kabul
Dubai
PAKISTAN
IRAN
NEPAL
INDIA
THAILAND
LAOS
Bay of Bengal
Bamako
Abidjan
Lagos
Kano
Yaounde
NIGERIA
CAMEROON
CHAD
NIGER
GHANA
BURKINA FASO
GABON
CONGO
DR CONGO
CENTRAL AFRICAN REPUBLIC

Figure 4.

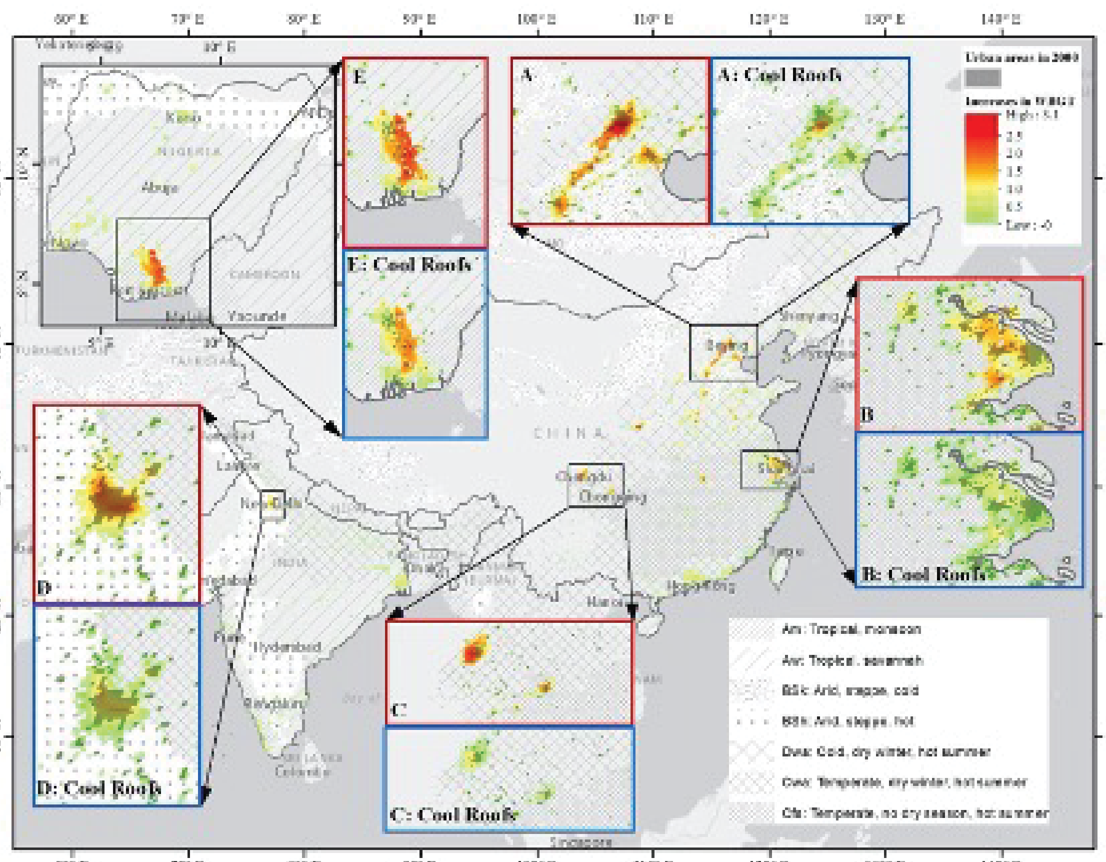

Urban areas in 2000
Increases in WBGT
High : 3.1
2.5
2.0
1.5
1.0
0.5
Low : -0
A
A: Cool Roofs
B
B: Cool Roofs
C
C: Cool Roofs
D
D: Cool Roofs
E
E: Cool Roofs
Am: Tropical, monsoon
Aw: Tropical, savannah
BSk: Arid, steppe, cold
BSh: Arid, steppe, hot
Dwa: Cold, dry winter, hot summer
Cwa: Temperate, dry winter, hot summer
Cfa: Temperate, no dry season, hot summer
Kano
NIGERIA
Abuja
CAMEROON
Yaounde
CHINA
Beijing
Shenyang
Shanghai
Chengdu
Chongqing
New Delhi
Lahore
INDIA
Pune
Hyderabad
Hanoi
Hong Kong
Colombo
Singapore

Figure 5.

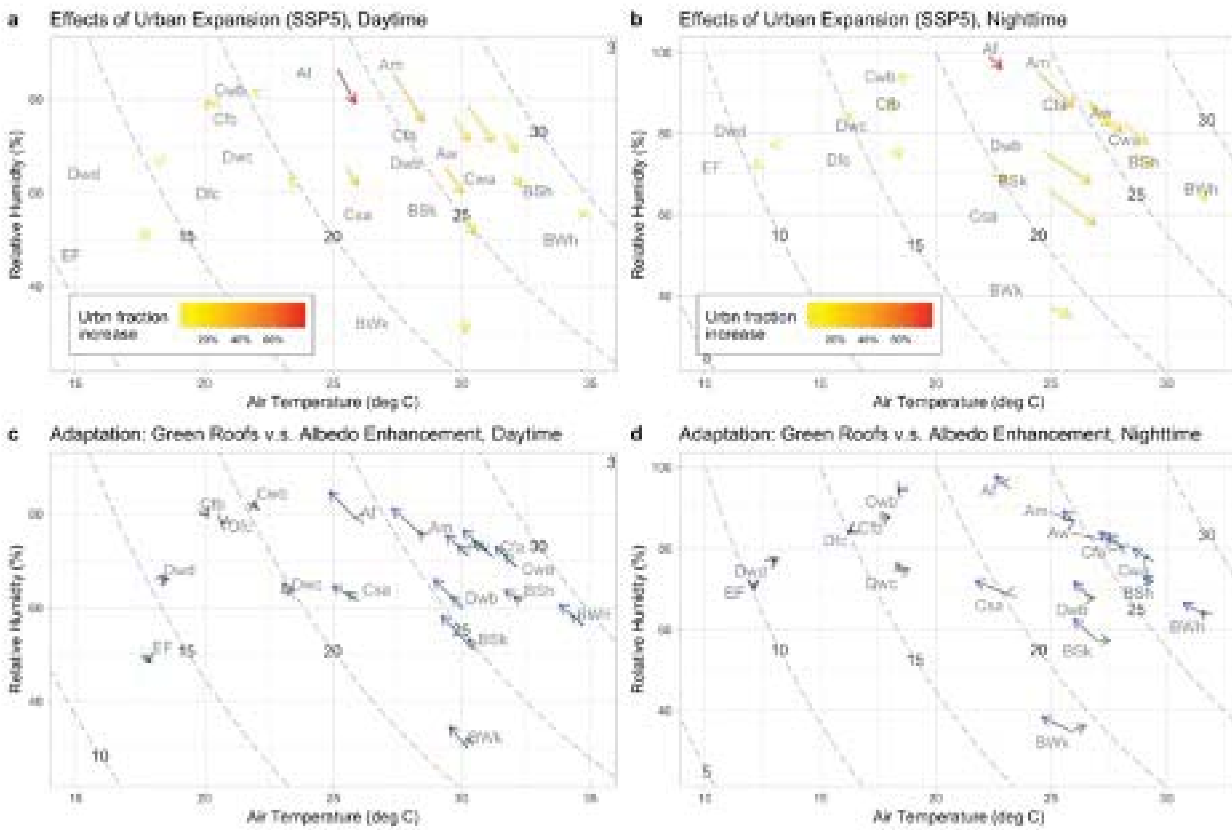

a
Effects of Urban Expansion (SSP5), Daytime
b
Effects of Urban Expansion (SSP5), Nighttime
c
Adaptation: Green Roofs v.s. Albedo Enhancement, Daytime
d
Adaptation: Green Roofs v.s. Albedo Enhancement, Nighttime
Relative Humidity (%)
Air Temperature (deg C)
Urbn fraction increase
Af
Am
Aw
BSh
BSk
BWh
BWk
Cfa
Cfb
Csa
Cwa
Dfc
Dwb
Dwc
Dwd
EF

Figure 3.

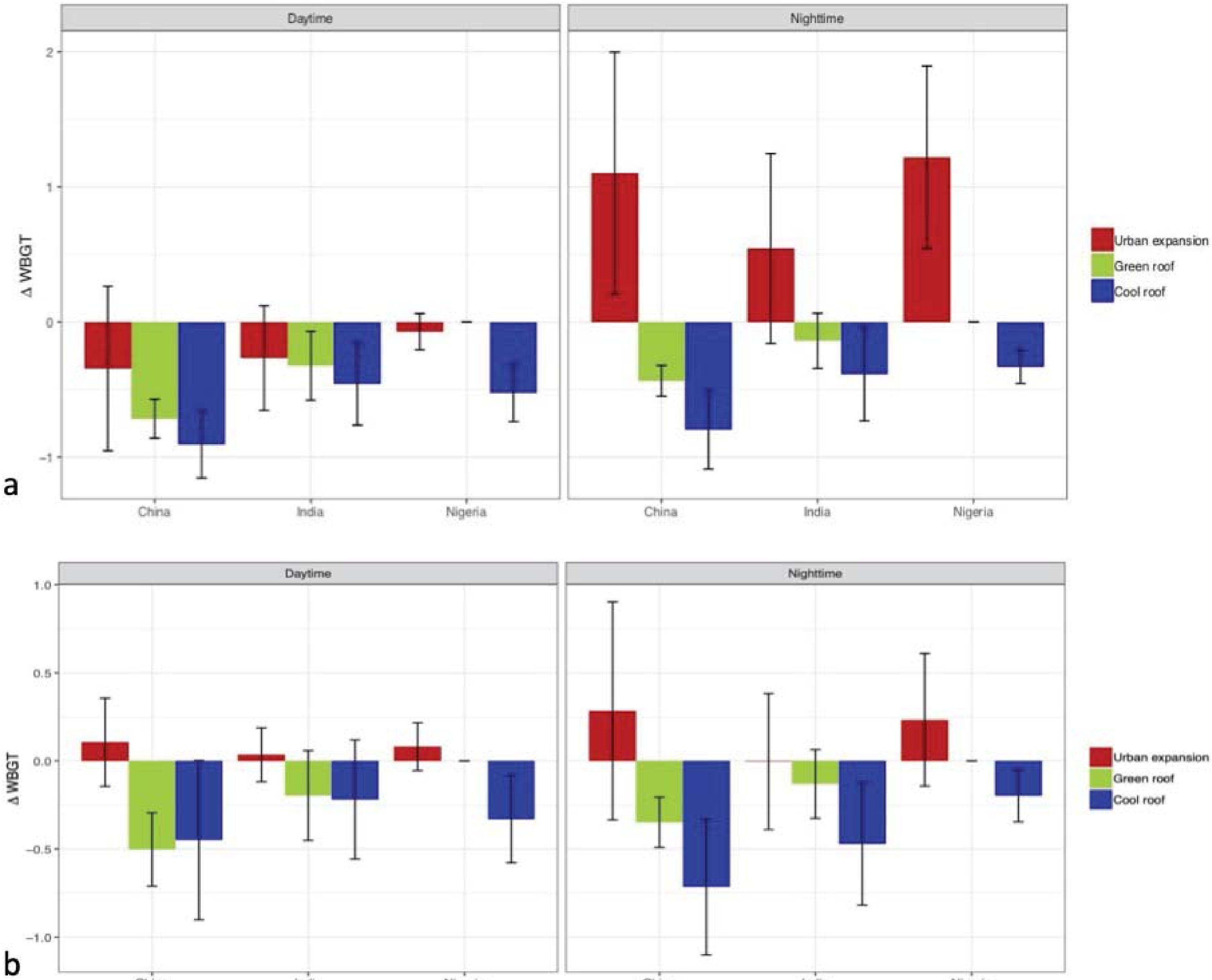
Daytime
Nighttime
Δ WBGT
2
1
0
−1
China
India
Nigeria
Urban expansion
Green roof
Cool roof
a
Daytime
Nighttime
Δ WBGT
1.0
0.5
0.0
−0.5
−1.0
China
India
Nigeria
Urban expansion
Green roof
Cool roof
b